International Journal on Magnetic Particle Imaging
Vol 8, No 2, Article ID 2210001, 10 Pages

Infinite Science Publishing

Research Article

VivoTrax+™ improves the detection of cancer cells with magnetic particle imaging

Julia J. Gevaert[a,b,*] · Kyle Van Beek[b] · Olivia C. Sehl[a,b] · Paula J. Foster[a,b]

[a]Department of Medical Biophysics, University of Western Ontario, Canada
[b]Cellular and Molecular Imaging Group, Robarts Research Institute, Canada
[*]Corresponding author, email: jgevaert@uwo.ca

Received 07 May 2022; Accepted 08 August 2022; Published online 22 October 2022

Abstract

Cellular imaging is a rapidly growing field as novel tracers and imaging techniques are developed. Magnetic particle imaging (MPI) detects superparamagnetic iron oxide (SPIO) particles, which can be used to label cells. The type of SPIO has a critical role in determining MPI sensitivity and resolution. For cell tracking applications, the ideal SPIO should label cells efficiently and retain its sensitivity after cellular uptake. VivoTrax™, a commercially available and commonly used SPIO for MPI, was recently re-released as VivoTrax+ with an improved size distribution enriched for larger particles. In this study, VivoTrax+ is shown to enhance cellular labeling and improve *in vitro/in vivo* sensitivity. Importantly, the sensitivity of both SPIO significantly decreased after cellular internalization. The results from this study emphasize the importance of translating SPIO performance *in vivo* to maintain its utility for cell tracking applications.

I. Introduction

Cellular imaging has the potential to answer many fundamental questions about the presence, numbers, persistence, and delivery of cell therapies. Magnetic particle imaging (MPI) is a non-invasive, non-ionizing, sensitive modality capable of tracking cells labeled with superparamagnetic iron oxide (SPIO) particles. Importantly, MPI signal is proportional to iron content, which, combined with a measure of iron per cell, can be used to quantify cell number. As a tracer-based modality, the type of SPIO has a critical role in determining sensitivity and resolution. The ideal SPIO for cell tracking should label cells efficiently and produce high MPI signal with good resolution.

VivoTrax™ (Magnetic Insight Inc.), or ferucarbotran, is a commercially available MPI tracer. Ferucarbotran has been used to detect a variety of cell types and as a comparison for newly synthesized particles [1–8]. Although widely used, it is not considered optimal for MPI due to its bimodal size distribution comprised of ~30% 25-30 nm cores and ~70% 5 nm cores [9, 10]. The smaller cores do not magnetize sufficiently, leaving a small fraction of particles that contribute to signal. Recently, Magnetic Insight released VivoTrax+, a magnetically fractionated form of VivoTrax that selects for the fraction of larger cores for improved MPI performance. To our knowledge, this is the first study that uses VivoTrax+ for cell tracking with MPI. The purpose of this study was to directly compare the two agents by assessing sensitivity, resolution, cell labeling efficiency, and *in vitro* and *in vivo* imaging, to determine if VivoTrax+ has improved MPI performance.

II. Methods

II.I. Cell Labeling

A2058 human melanoma cancer cells were cultured at 37° in complete Dulbecco's modified Eagle's medium (DMEM) (Thermo Fisher Scientific, Waltham, Massachusetts) until 90% confluent. For both VivoTrax+ and VivoTrax, labeling was done with and without protamine sulfate and heparin as transfection agents (TAs). For the cells labeled with TAs, 60 µL of protamine sulfate (stock 10 µg/µL) and 20 µL of heparin (stock 1 U/µL) were added to culture with 90 µL of either VivoTrax or VivoTrax+ (stock 5.5 µg Fe/µL) in 5 mL of serum-free DMEM. After 4 hours of incubation, 5 mL of complete DMEM was added to culture for a total volume of 10 mL in T75 cm^2 flasks. For the cells labeled without TAs, 90 µL of either VivoTrax or VivoTrax+ was added to culture in a total volume of 10 mL complete DMEM in T75 cm^2 flasks. All flasks were incubated overnight after which cells from each flask were collected and washed 3 times with phosphate-buffered saline (PBS). Cell counting and viability was determined using the trypan-blue exclusion assay (Countess Automated Cell Counter; Invitrogen). Perls Prussian Blue (PPB) staining was then performed to assess iron labeling [11].

For cells labeled with TAs, Ficoll-Pacque density gradient separation was applied to remove unwanted, extracellular iron that remained after PBS washing. Cells were suspended in 6 mL media and carefully layered over 3 mL Ficoll-Pacque in a 15 mL falcon tube then spun at 400 × g for 20 minutes without brakes. Cells were collected at the interface of the two solutions, then separation of labeled from unlabeled cells was conducted with a magnetic column. Cells were resuspended in 2 mL PBS and incubated for 5 minutes in an EasySep™ magnet (Stemcell Technologies, Vancouver, CAN) at room temperature. Flow through of unlabeled cells was discarded while SPIO-labeled cells remaining in the tube were collected.

At each labeling stage (before Ficoll-Pacque, after Ficoll-Pacque, and after magnetic column separation), PPB staining was performed and samples containing 1×10^6 cells suspended in ~250 µL PBS were collected for MPI acquisitions. Only cells labeled with TAs were used for further experiments.

II.II. MPI Relaxometry

MPI relaxometry was performed for VivoTrax and VivoTrax+ as (i) free SPIO and (ii) intracellular SPIO. For free SPIO, triplicate samples containing 3 µL (5.5 µg Fe/ µL) of each agent were prepared (n = 3 VivoTrax, n = 3 VivoTrax+). For intracellular SPIO, triplicate samples containing 1×10^6 VivoTrax+ or VivoTrax labeled cells from each labeling stage (before Ficoll-Pacque, after Ficoll-Pacque, and after magnetic separation) were prepared (n = 3 VivoTrax labeled cells, n = 3 VivoTrax+ labeled cells). Samples were individually scanned using the RELAX™ module equipped on the Momentum™ scanner (Magnetic Insight Inc.), producing a point spread function (PSF) for each sample. PSF's were analyzed using Prism software (9.3.0, GraphPad Inc.) for signal (peak height) and resolution (full width half maximum – FWHM).

First, the relaxometry curves for free agents were compared. To assess sensitivity, the curves were normalized to the amount of iron in each sample, and to visually assess PSF resolution, the curves were normalized to the maximum signal value.

Next, relaxometry curves from SPIO-labeled cells at each labeling stage were compared. Since these samples have the same number of cells, no PSF normalization was conducted when assessing sensitivity. Therefore, differences in peak signal may be attributed to differences in the amount of iron associated with the cell samples.

Lastly, the effects of cellular internalization were studied by comparing PSF signal and resolution of (i) free VivoTrax+ vs. intracellular, (ii) free VivoTrax vs. intracellular, and (iii) intracellular VivoTrax+ vs. VivoTrax. For these comparisons, PSFs were normalized to the amount of iron in the sample (signal) or to the maximum value (resolution). The intracellular data was taken from labeled cell samples after magnetic column separation.

II.III. *In vitro* MPI Acquisitions

Samples containing 62.5k, 31.3k, 15.6k, 7.8k, and 3.9k (k = 1000) VivoTrax+ or VivoTrax labeled cells suspended in ~250 µL PBS were prepared from each labeling stage. Projection images were acquired in 2D with a 3.0 T/m selection field gradient and drive field strengths of 22 mT and 26 mT in the X and Z axes, respectively. These 2D images took ~2 minutes to acquire for a 12 x 6 cm field of view (FOV). These *in vitro* acquisitions were performed for two purposes: (i) to assess the effects of extracellular iron on MPI signal after being removed by Ficoll-Pacque and magnetic column separation, and (ii) to compare the cell detection sensitivities of VivoTrax+ and VivoTrax.

II.IV. *In vivo* MPI Acquisitions

In vivo imaging was performed on nude mice 24 hours post intravenous (IV) injections of 40 µL (220 µg Fe) VivoTrax+ (n = 3) and VivoTrax (n = 3). Prior to imaging, mice were fasted for 12 hours with only water, a laxative, and corn bedding in their cage to reduce gastrointestinal signal. Mice were anesthetized with 2% isoflurane and maintained with 1% isoflurane during imaging. The same image parameters were used for 3D imaging, which combines 35 projections (~30 min).

10.18416/ijmpi.2022.2210001

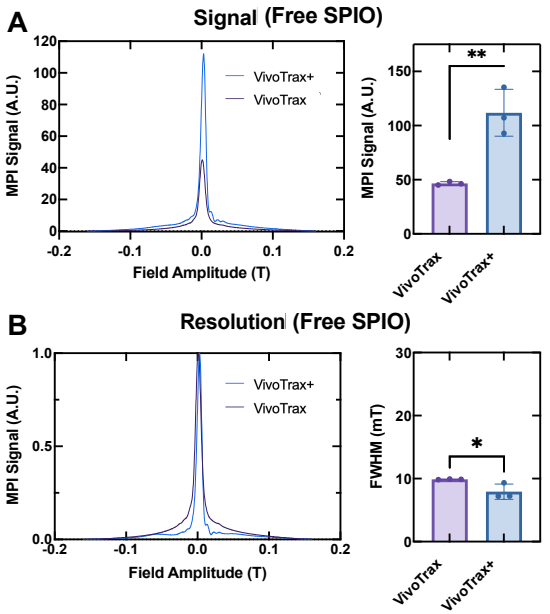

Figure 1: MPI relaxometry data comparing free VivoTrax+ and VivoTrax. (a) MPI signal was 2.4 times higher for VivoTrax+ compared to VivoTrax. (b) VivoTrax+ improved resolution by 1.3 times compared to VivoTrax. (unpaired t-tests, * - $p \leq 0.05$, ** - $p \leq 0.01$).

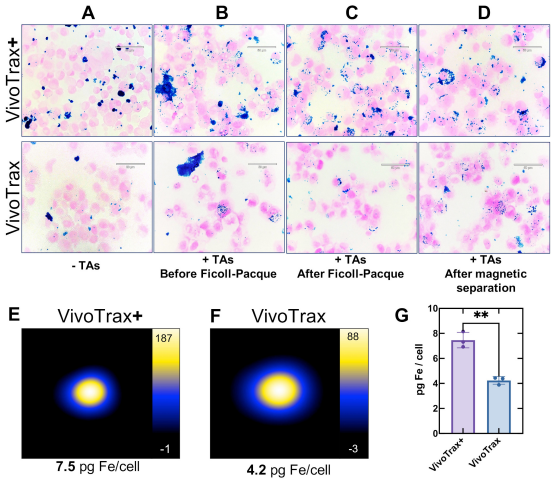

Figure 2: PPB of A2058 cancer cells labeled with VivoTrax+ and VivoTrax (a) without TAs (b) with TAs before Ficoll-Pacque (c) after Ficoll-Pacque and (d) after magnetic separation. 2D images of 1×10^6 labeled cells with (e) VivoTrax+ had an average of 7.5 pg Fe/cell and (f) VivoTrax had an average of 4.2 pg Fe/cell. (g) Iron content per cell was higher for VivoTrax+ compared to VivoTrax (unpaired t-tests, ** - $p \leq 0.01$).

II.V. Image Quantification and Statistics

All MPI images were imported and viewed with a custom MPI colour look-up table (CLUT) using the open-source Horos™ image analysis software (version 3.3.6, Annapolis, MD USA). MPI signal was measured within a specific region of interest (ROI) for both 2D and 3D images that selects for signal 5 times above the standard deviation of the background noise. Total MPI signal for the ROI was calculated by multiplying the ROI area (2D) or volume (3D) by the mean signal. The signal to noise ratio (SNR) was calculated by dividing the mean signal for the ROI by the standard deviation of the background noise. The SNR had to be greater than 5 for the MPI signal to be considered detectable and for images to be further quantified [12]. All MPI images were delineated and analyzed in the same way to ensure consistency. To calculate iron content per cell, samples containing 1×10^6 labeled cells (after magnetic column separation) were used to produce high SNR image data for quantification of iron mass using calibration lines [4, 13]. To determine pg/cell, this iron mass was divided the by the number of cells in the cell pellet.

The relationship between MPI signal (and therefore iron content) and cell number was determined by performing a simple linear regression. Unpaired t-tests were used to compare relaxometry results between free and intracellular SPIO. Ordinary one-way ANOVA tests were used to compare relaxometry results between the 1×10^6 labeled cell samples taken from the three labeling stages.

III. Results and discussion

III.I. VivoTrax+ has higher signal and resolution than VivoTrax as a free SPIO

Figure 1 shows the PSFs obtained from MPI relaxometry for free VivoTrax+ and VivoTrax. The peak signal was significantly higher (2.4 times) for VivoTrax+ compared to VivoTrax after normalizing the signal to the amount of iron in each sample (111.8 vs. 46.6 A.U., $p \leq 0.01$) (Figure 1a). Resolution improved by 1.3 times for VivoTrax+ over VivoTrax, indicated by a decreased FWHM after normalizing to the maximum signal per amount of iron (7.9 mT vs 9.9 mT, $p \leq 0.05$, Figure 1b). For imaging with a 3.0 T/m gradient strength, FWHM = 7.9 mT is expected to provide a resolution of 2.63 mm and FWHM = 9.9 mT a resolution of 3.3 mm.

III.II. Cell labeling is more efficient with VivoTrax+

Without TAs, most iron remained extracellular with minimal uptake in cancer cells for both VivoTrax+ and VivoTrax (Figure 2a). The use of TAs enhanced iron uptake in these less phagocytic cells but also produced extracellular clusters of iron (Figure 2b). Ficoll-Pacque efficiently

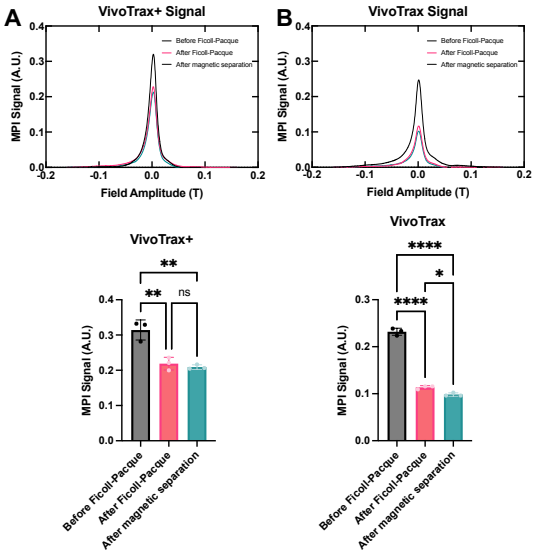

Figure 3: Relaxometry showing the signal of labeled cells before and after Ficoll-Pacque and after magnetic column separation for (a) VivoTrax+ and (b) VivoTrax. (Ordinary one-way ANOVA, ns – $p > 0.05$, * - $p \leq 0.05$, ** - $p \leq 0.01$, *** - $p \leq 0.001$, **** - $p \leq 0.0001$).

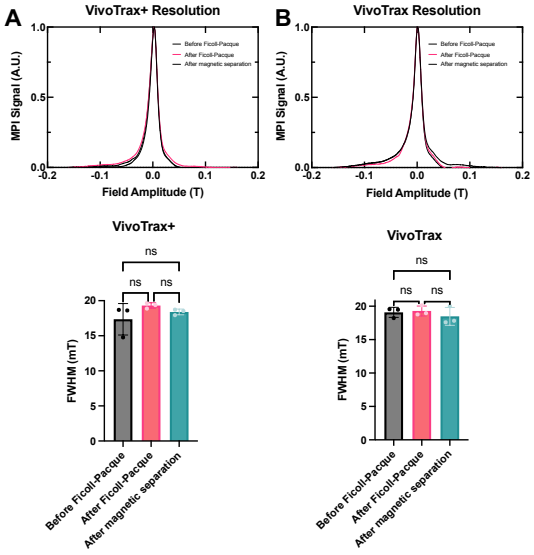

Figure 4: Relaxometry showing the resolution of labeled cells before and after Ficoll-Pacque and after magnetic column separation for (a) VivoTrax+ and (b) VivoTrax. (Ordinary one-way ANOVA, ns – $p > 0.05$).

removed extracellular iron (Figure 2c). After magnetic separation, unlabeled cells were removed (Figure 2d). Visually, panels (c) and (d) are similar indicating most cells were labeled and few were removed after magnetic separation. Qualitatively, VivoTrax+ improved uptake in cells compared to VivoTrax. Cell viability was high after labeling with either agent (VivoTrax+ – 91%, VivoTrax – 92%). Quantitative measurements with MPI indicate that cells labeled with VivoTrax+ had an average of 7.5 pg Fe/cell (Figure 2e) and cells labeled with VivoTrax had an average of 4.2 pg Fe/cell (Figure 2f). Iron per cell was significantly higher for VivoTrax+ compared to VivoTrax™ ($n = 3$, $p \leq 0.01$).

III.III. Extracellular iron affects MPI signal

After Ficoll-Pacque, the MPI signal produced from cell pellets of 1×10^6 cells decreased by ~33% for VivoTrax+ labeled cells ($p \leq 0.01$, Figure 3a) and ~50% for VivoTrax labeled cells ($p \leq 0.0001$, Figure 3b) because of the removal of the extracellular iron. For these relaxometry curves, signal was not normalized to iron to show the effects of extracellular iron on signal between samples containing the same number of cells (1.0×10^6). This result shows the extent to which contamination of cell samples with extracellular iron will lead to an overestimation of the MPI signal associated with cells, and ultimately of cell detection sensitivity and specificity as free SPIO may be taken up by bystander cells *in vivo*. Thus, the Ficoll-Pacque technique may be critical for accurate detection and quantification from images of labeled cells.

For VivoTrax+ labeled cells, there was no significant change in MPI signal after magnetic separation, indicating few cells were unlabeled. With VivoTrax, there was a small reduction in MPI signal after magnetic separation ($p \leq 0.01$). This result could be explained by VivoTrax having a larger fraction of smaller cores that were loosely bound and not internalized by cells, which were removed by the magnetic column resulting in a small drop in signal [14].

MPI resolution was also assessed by evaluating the FWHM values from the PSF at each cell labeling stage. Across all three labeling stages, there were no significant changes in resolution for either VivoTrax+ (Figure 4a) or VivoTrax (Figure 4b).

III.IV. Cellular internalization affects signal and resolution

MPI signal from free vs. intracellular SPIO was assessed using MPI relaxometry, shown in Figure 5. After cellular internalization, the peak MPI signal was significantly reduced for both SPIO (Figure 5a). The PSF signal for intracellular VivoTrax+ was 4.3 times lower than the signal for free VivoTrax+ (111.8 vs. 26.0 A.U., $p < 0.01$, Figure 5b). The PSF signal for intracellular VivoTrax was 2.3 times lower than the signal for free VivoTrax (46.6 vs 20.3 A.U., $p < 0.0001$, Figure 5c). Therefore, cellular internalization of VivoTrax+ and VivoTrax significantly reduced the MPI sensitivity.

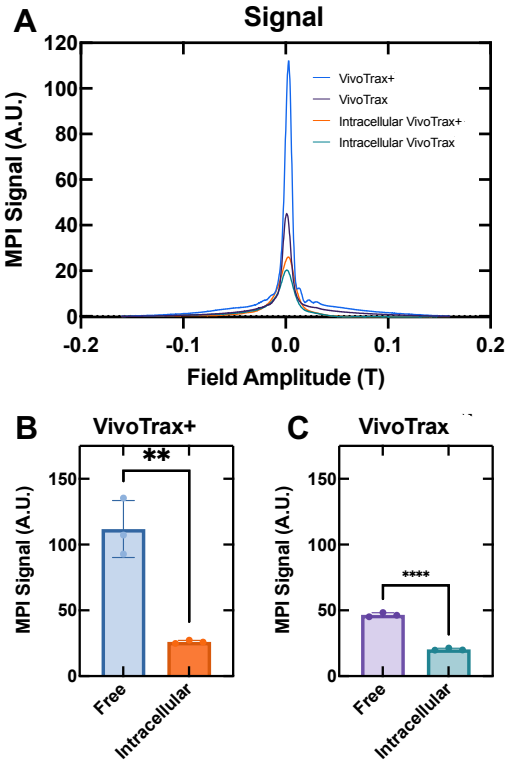

Figure 5: (a) PSF's showing peak MPI signal from relaxometry for free and intracellular VivoTrax+ and VivoTrax. (b) VivoTrax+ signal was reduced by 4.3 times after cellular internalization. (c) VivoTrax signal was reduced by 2.3 times after cellular internalization. (unpaired t-tests, ** - $p \leq 0.01$, **** - $p \leq 0.0001$).

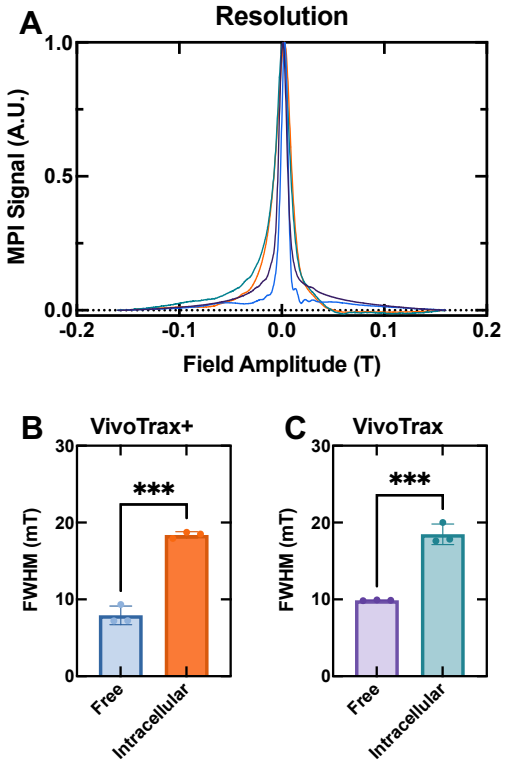

Figure 6: (a) PSF's showing resolution from MPI relaxometry for free and intracellular VivoTrax+ and VivoTrax. (b) Resolution was reduced by 2.3 times after cellular internalization for VivoTrax+ and (c) reduced by 1.9 times after cellular internalization for VivoTrax. (unpaired t-tests, *** - $p \leq 0.001$).

The relaxometry signal from cells labeled with VivoTrax+ was significantly higher (1.3 times) than cells labeled with VivoTrax (26 A.U. vs. 20.3 A.U., $p \leq 0.01$). This important result shows that the substantial signal gain in sensitivity when comparing the free tracer (see Part III.I) does not fully translate after cellular uptake. As free SPIO, VivoTrax+ produces 2.4 times more signal than VivoTrax; however, in cells the relaxometry signal is only 1.3 times higher.

Intracellular resolution was also assessed using MPI relaxometry shown in Fig. 6. After cellular internalization, resolution decreased for both SPIO (Figure 6a). The resolution for VivoTrax+ labeled cells was 2.3 times lower after cellular internalization, indicated by an increase in FWHM from 7.9 mT to 18.4 mT ($p \leq 0.001$, Figure 6b). The resolution for VivoTrax labeled cells was 1.9 times lower after cellular internalization with an increase of FWHM from 9.9 mT to 18.5 mT ($p \leq 0.001$, Figure 6c). The improved resolution observed for free VivoTrax+ over free VivoTrax was lost after cell labeling; there was no significant difference in FWHM values between the SPIO after cellular internalization (18.4 mT vs 18.5 mT, $p > 0.05$). Overall, although VivoTrax+ demonstrated improved MPI signal and resolution measured by MPI relaxometry as a free tracer, these improvements do not translate after cellular internalization.

III.V. VivoTrax+ improves cell detection in images

2D images of cell samples are shown in Figure 7 with the total MPI signal (ROI area × mean signal) beneath. As few as 15.6K VivoTrax+ labeled cells were detected after all 3 labeling stages (Figure 7a-c). With VivoTrax, 15.6K cells could be detected before Ficoll-Pacque, likely because of extracellular iron contributing to MPI signal (Figure 7d). After extracellular iron was removed, the signal in images decreased, and the lowest cell number detected was 31.3K cells (Figure 7e). After magnetic separation, there was a slight decrease in signal, and only as few as 62.5K cells were detected (Figure 7f). This may be explained by the column removing cells with extracellular iron bound to their surface. If these cells were removed by the column, the remaining cells would have lower iron mass which would lower sensitivity.

This experiment showed that less iron and ~4 times fewer cells were detected with VivoTrax+ compared to VivoTrax. Importantly, the extracellular iron present

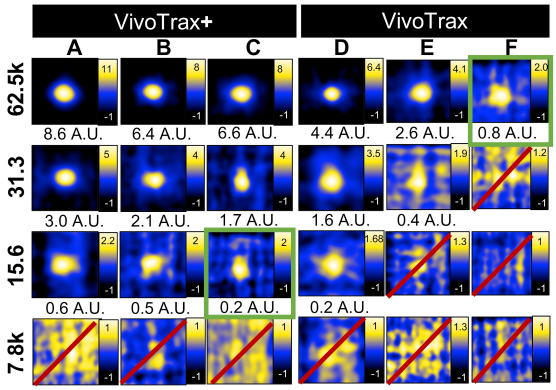

Figure 7: 2D MPI of cell samples (a, d – before Ficoll-Pacque, b, e – after Ficoll-Pacque, c, f – after magnetic separation). After magnetic column separation, as few as 15.6K cells were detected with VivoTrax+ and 62.5K cells with VivoTrax (indicated by the green boxes). Red lines indicate signal that was below the detection threshold. Total MPI signal (ROI area × mean signal) is shown below images.

in the cell samples prior to Ficoll-Pacque falsely contributed to the signal in images with VivoTrax, overestimating detection sensitivity.

Strong linear relationships ($R^2 > 0.97$) between cell number and MPI signal were observed for both SPIO (Figure 8). The slope of the lines significantly decreased ($p \leq 0.0001$) after Ficoll-Pacque separation, which is consistent with the reduction in MPI signal seen with *in vitro* images (Figure 7). Removal of extracellular iron with Ficoll-Pacque separation reduces unwanted "false" MPI signals, providing a more accurate measure of MPI signal from labeled cells.

III.VI. *In vivo* cell detection is improved with VivoTrax+

Six nude mice were imaged with MPI following IV injected VivoTrax+ (n = 3) or VivoTrax (n = 3) and positioned as shown in Figure 9a. MPI signal was observed in the mouse liver 24 hours post-injection, resulting from uptake of iron by phagocytic Kupffer cells (liver macrophages). The MPI signal was significantly higher (1.4 times, 177.5 A.U. vs. 129.7 A.U.) in the livers of mice injected with VivoTrax+ compared to VivoTrax (Figure 9b). *In vivo* images for mice injected VivoTrax+ are shown in Figure 9c and VivoTrax in Figure 9d. Residual iron from the injection is seen in the tail for Mouse 2 (Figure 9d).

The presence of VivoTrax+ in the liver was validated *ex vivo* with PPB staining of fixed sections (Figure 10). The blue in the images indicates the presence of iron, with the cells counterstained with Nuclear Fast red.

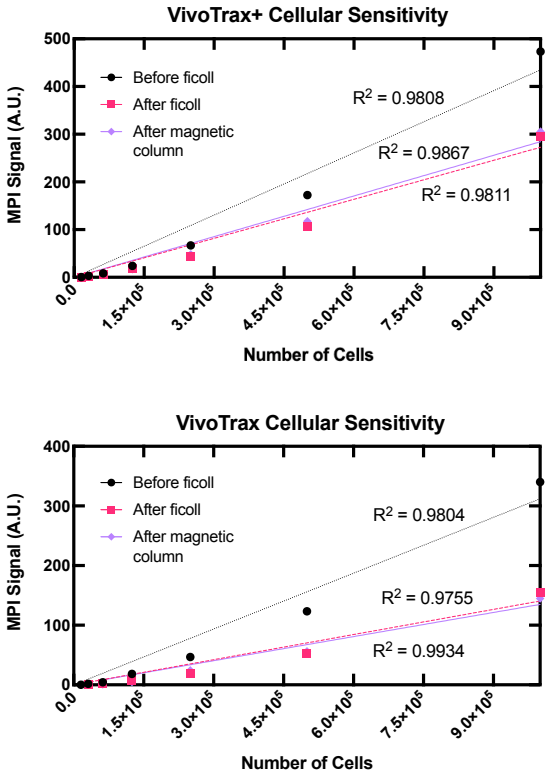

Figure 8: Cellular sensitivity lines for VivoTrax+ and VivoTrax show a linear relationship ($R^2 > 0.97$) between MPI signal (iron content) and cell number.

IV. Discussion

One of the main findings of this study was that the PSF for free VivoTrax+ had a higher peak signal (2.4 times) and better resolution (1.3 times) when compared to VivoTrax. This result was expected since core size and distribution affect the spatial resolution and sensitivity of the MPI signal [15]. We speculate that the magnetic fractionation of the ferucarbotran (VivoTrax) formulation reduces the polydispersity and enhances the percentage of larger multicore clusters, which contribute more significantly to MPI signal. According to manufacturer reported values, the mean core size for VivoTrax and VivoTrax+ are 4 nm and 6 nm, respectively. Mean core size is not representative of the shape of the size distribution. Although small, this shift in mean core size can have a large impact on the ensemble average of the magnetic properties. This is supported by quantifiable improvements in signal and resolution measurements. This approach had been taken before by Yoshida *et al.* with ferucarbotran (Resovist), who separated ferucarbotran into three fractionated nanoparticles, with effective core sizes of 21.6 nm, 10.7 nm and 6.2 nm [16]. The 21.6 nm particles alone showed an increase of 2.5 times in the third harmonic signal compared to Resovist, in excitation fields of 2.8 mT and 28 mT. This agrees with our result of VivoTrax+ hav-

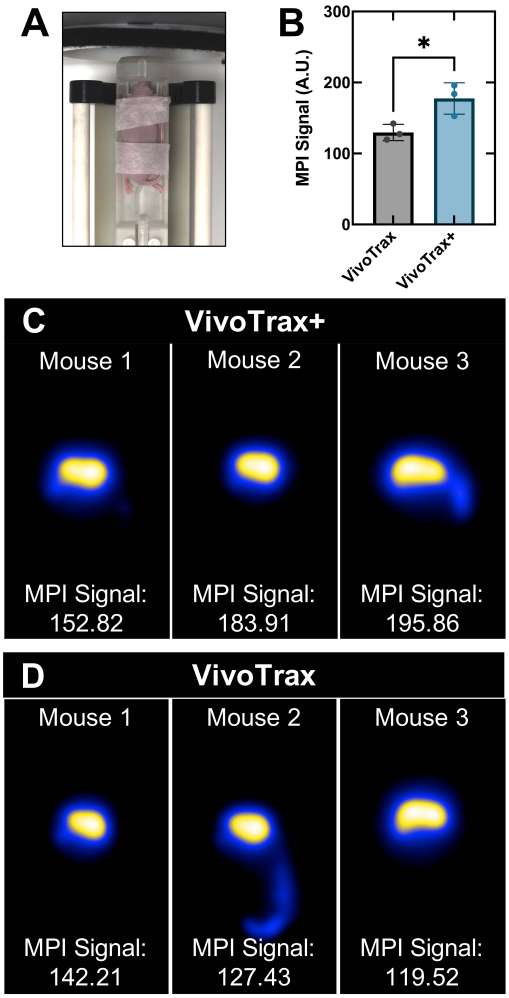

Figure 9: *In vivo* MPI signal of VivoTrax+ and VivoTrax after IV injections in nude mice. (a) Experimental set-up for *in vivo* imaging. (b) Significantly more signal (1.4 times) was detected in mice injected with VivoTrax+ than VivoTrax. 3D MPI images are shown of nude mice IV injected with (c) VivoTrax+ and (d) VivoTrax.

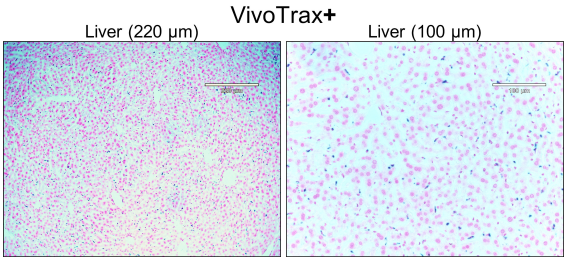

Figure 10: PPB stains from liver sections of a representative mouse IV injected with VivoTrax+.

ing 2.4 times more signal compared to VivoTrax. The 10.7 nm fraction exhibited almost the same spectrum as Resovist, and the 6.2 nm sampled showed a smaller harmonic spectrum. These findings demonstrate the role of iron core size and distribution in generating MPI signal. Lowa *et al.* compared two methods for fractionating Resovist; asymmetric flow field-field fractionation (A4F) and static magnetic fractionation (SMF) [17]. They verified the presence of a broad hydrodynamic size and anisotropy energy distribution for Resovist, in agreement with previous studies [16, 18]. For both fractionation methods, the third harmonic signal increased up to 220% for the larger-sized fractions. This is in line with our finding of 2.4 times more signal for free VivoTrax+. They also showed that the larger-sized fraction produced by SMF had a broader hydrodynamic size distribution and larger anisotropy energy compared to all other fractions obtained by A4F. They conclude that in SMF, the column retains the nanoparticles with larger magnetic moments (and thus lower contributions of Neel relaxation), while in A4F, nanoparticles are selected by size only.

A second major finding from this work was that the intracellular MPI signal was significantly reduced compared to free SPIO. Although fractionation resulted in higher MPI signal for free Vivotrax+, this did not hold once intracellular. MPI relaxometry showed that the peak signal was 2.4 times higher for free Vivotrax+, however in cells the signal was only 1.3 times higher. This result agrees with previous studies which have shown that after cellular internalization the magnetic properties of SPIOs deteriorate leading to lower MPI signal and resolution. This is thought to be related to aggregation [19, 20], immobilization [21], compartmentalization [19], or the viscosity [22, 23] of the iron cores which impact the Neel and Brownian relaxation dynamics.

Teeman *et al.* showed a 20% reduction in signal after their particles were internalized in human cancer cells and determined that this was the result of magnetostatic interactions between particles, which limits their ability to interact with the applied magnetic field, and not due to changes in the physical characteristics of particle or the viscosity of the surrounding environment [24]. Markov *et al.* compared Resovist and Sineram for labeling red blood cells (RBCs), using transient membrane poration induced by changing the cell osmolarity, and reported that the MPS signal was reduced by approximately 8 times for Resovist and by 4 times for Sinerem, after RBC encapsulation [25]. Electron microscopy revealed a uniform non-aggregated distribution inside of RBCs. Instead, the signal reduction was attributed to size selectivity in RBC loading resulting in a preferential encapsulation of smaller nanoparticles with a mean core diameter of 4–7 nm, which are not ideal for MPI signal generation. This was more pronounced for Resovist because it contains more larger particles.

Suzuka *et al.* showed that changes in the magnetic behaviour of particles after cell labeling was different for different cell types [19]. There are several important results from their study that are relevant to this present

study. First, they showed that labeling with TAs enhanced the uptake of Resovist by non-phagocytic colon cancer cells and increased the signal in MPI images. In our study, TAs were also necessary to increase uptake in melanoma cancer cells. We both used a cationic TA, protamine sulfate (PS), which has been previously shown to facilitate the labeling of cells with iron particles [14, 26, 27]. This involves forming iron-PS nanocomplexes which are added to the media in the cell culture, which reverses the negative charge of the nanoparticles allowing them to interact with the negatively charged cell membrane. Crosslinking can occur between TAs and multiple nanoparticles, creating large clusters observable using light microscopy [14]. As the size of the complex increases, there is the potential for adherence of complexes to cell membrane surfaces and large complexes will remain extracellular. Second, they showed that the use of TAs increased the hydrodynamic diameter of the nanoparticles and inhibited the MPI signal. We have also observed a reduction in the peak signal of the PSF when comparing iron particles in solution and iron particles mixed with TAs [28]. Third, Suzuka *et al.* compared the MPI signal for cancer cells labeled using TAs and for macrophages which are naturally highly phagocytic and do not need TAs for labeling. The signal reduction was greater for cancer cells compared to macrophages. Electron microscopy revealed that the nanoparticles were aggregated in cancer cells but not in macrophages. Furthermore, in macrophages they were located on the inner surface of the cell compartments, whereas in cancer cells, they were aggregated at the center of the endosomes. This indicates different modes of endocytosis. Both the higher amount of aggregation and the increase in hydrodynamic size, caused by the use of TAs for labeled cancer cells, likely led to the greater reduction in MPI signal. In either case, cell lysis restored the MPI suggesting that the signal loss was induced, at least in part, by the cellular uptake itself.

In this paper we show that the use of TAs to label cells can lead to iron clusters and overestimation of the total amount of iron if they are not removed. We separated cancer cells from extracellular iron using density gradient centrifugation and sorted for labeled cells using magnetic separation. Cells labeled with VivoTrax showed more extracellular iron compared to those labeled with VivoTrax+. In the final cell preparation, cells labeled with VivoTrax+ contained more iron/cell than those labeled with VivoTrax. MPI relaxometry of cell samples showed that after Ficoll-Pacque, the peak signal decreased by ~33% for VivoTrax+ labeled cells and ~50% for VivoTrax labeled cells due to the removal of extracellular iron. Quantification from images of cell samples also showed a significant reduction in the MPI signal and detection sensitivity of cell samples. Figure 7 clearly shows that for cell samples imaged after Ficoll-Pacque and magnetic separation (columns C and F) the MPI signal from images was much higher for VivoTrax+ and, as a result, fewer cells could be detected. Both the higher loading and lower level of extracellular iron for VivoTrax+ likely led to this improvement in cell detection sensitivity.

In summary, the decreased MPI signal we observed from SPIO after cell labeling may be explained by a combination of factors. First, the use of TAs may have caused increased aggregation, leading to an overall larger hydrodynamic size, and slowing relaxation. Second, after internalization, there may have been increased magnetostatic interactions between SPIO accumulating inside the cells, also slowing relaxation. Ultimately, decreased signal after internalization will depend on the SPIO, cell type, and labeling strategy used, caused by a combination of factors affecting the magnetic relaxation mechanisms of SPIO in the intracellular environment.

In some cases, the change in MPI signal when SPIO is in different environments may be useful. For example, Paysen *et al.* demonstrated that the difference in signal between free and intracellular Synomag could be separated and they used an extended MPI image reconstruction technique which allowed the visualization and quantification of the cellular uptake of Synomag by THP-1 cells [29]. Another application that benefits from the differences in SPIO signal is colour MPI, which separates signals acquired simultaneously from different particle types or from particles in different environments. Different colors could then be assigned to different signal sources to allow for visualization in a single image [30].

In vivo the signal from SPIO uptake by liver macrophages following intravenous administration was 1.4 times higher for VivoTrax+ than VivoTrax. This is similar to the *in vitro* relaxometry measurements that showed VivoTrax+ labeled cancer cells produce 1.3 times more signal than VivoTrax labeled cells; however, compared to the *in vitro* MPI images, VivoTrax+ enabled detection of ~4 times fewer cells. This difference may be explained by the difference in how signal is acquired and measured between relaxometry and images. Relaxometry quantifies the peak signal, and this was done using a sample containing 1.0×10^6 labeled cells with a high SNR. For imaging, the integrated signal within a ROI is quantified by multiplying the ROI area by the mean signal intensity, and this was done using cell numbers close to the detection limit with low SNR. Overall, VivoTrax+ is beneficial for cell tracking by having a larger fraction of iron cores that contribute more to MPI signal and by labeling melanoma cancer cells more efficiently leading to a higher cellular sensitivity with MPI.

V. Conclusions

This study compares VivoTrax+ and VivoTrax as MPI tracers and their potential use for cell tracking applications. Signal and resolution were compared using MPI relaxometry by measuring peak signal and FWHM values from

PSF's for both free and intracellular SPIO. As a free SPIO, VivoTrax+ had significantly higher signal (2.4 times) and resolution (1.3 times). VivoTrax+ had a higher labeling efficiency compared to VivoTrax (7.5 pg Fe/cell vs. 4.2 pg Fe/cell) using transfection agents as a labeling strategy to enhance cellular uptake. After cellular internalization, signal was reduced by 4.3 times for VivoTrax+ and 2.3 times for VivoTrax from changes in the local cellular environment affecting magnetic relaxation. Intracellularly, VivoTrax+ had higher signal (1.3 times) than VivoTrax measured by relaxometry and detected ~4 times fewer cells from *in vitro* MPI images. We demonstrate a significant decrease in signal for both SPIOs after cellular internalization and the importance of removing extracellular iron using a density gradient technique for accurate detection of cells. Furthermore, a higher cellular sensitivity was achieved *in vivo* with significantly more MPI signal detected in the liver of nude mice 24 hours post IV SPIO-injection. This study emphasizes two important factors to consider when developing MPI-tailored SPIO for the purposes of cell tracking: (i) ideally SPIO should retain their magnetic properties after cellular internalization and (ii) SPIO should efficiently label cells with high quantities of iron per cell and minimal extracellular iron. Overall, this study demonstrates a comprehensive analysis of SPIOs designed for MPI and their utility in cell tracking by evaluating their magnetic relaxation, cellular labeling efficiency, and *in vitro* and *in vivo* signal.

Acknowledgments

We acknowledge funding from the National Sciences and Engineering Research Council.

Author's statement

Conflict of interest: Authors state no conflict of interest.

References

[1] J. W. M. Bulte, P. Walczak, M. Janowski, K. M. Krishnan, H. Arami, A. Halkola, B. Gleich, and J. Rahmer. Quantitative "Hot-Spot" Imaging of Transplanted Stem Cells Using Superparamagnetic Tracers and Magnetic Particle Imaging. *Tomography*, 1(2):91–97, 2015, doi:10.18383/j.tom.2015.00172.

[2] A. V. Makela, J. M. Gaudet, M. A. Schott, O. C. Sehl, C. H. Contag, and P. J. Foster. Magnetic Particle Imaging of Macrophages Associated with Cancer: Filling the Voids Left by Iron-Based Magnetic Resonance Imaging. *Molecular Imaging and Biology*, 22(4):958–968, 2020, doi:10.1007/s11307-020-01473-0.

[3] A. Rivera-Rodriguez, L. B. Hoang-Minh, A. Chiu-Lam, N. Sarna, L. Marrero-Morales, D. A. Mitchell, and C. M. Rinaldi-Ramos. Tracking adoptive T cell immunotherapy using magnetic particle imaging. *Nanotheranostics*, 5(4):431–444, 2021, doi:10.7150/ntno.55165.

[4] K. P. Melo, A. V. Makela, N. N. Knier, A. M. Hamilton, and P. J. Foster. Magnetic microspheres can be used for magnetic particle imaging of cancer cells arrested in the mouse brain. *Magnetic Resonance in Medicine*, 87(1):312–322, 2022, doi:10.1002/mrm.28987.

[5] Q. Wang, X. Ma, H. Liao, Z. Liang, F. Li, J. Tian, and D. Ling. Artificially Engineered Cubic Iron Oxide Nanoparticle as a High-Performance Magnetic Particle Imaging Tracer for Stem Cell Tracking. *ACS Nano*, 14(2):2053–2062, 2020, doi:10.1021/acsnano.9b08660.

[6] P. Wang, P. W. Goodwill, P. Pandit, J. Gaudet, A. Ross, J. Wang, E. Yu, D. W. Hensley, T. C. Doyle, C. H. Contag, S. Conolly, and A. Moore. Magnetic particle imaging of islet transplantation in the liver and under the kidney capsule in mouse models. *Quantitative Imaging in Medicine and Surgery*, 8(2):114–122, 2018, doi:10.21037/qims.2018.02.06.

[7] B. Zheng, T. Vazin, P. W. Goodwill, A. Conway, A. Verma, E. Ulku Saritas, D. Schaffer, and S. M. Conolly. Magnetic Particle Imaging tracks the long-term fate of in vivo neural cell implants with high image contrast. *Scientific Reports*, 5(1):14055, 2015, doi:10.1038/srep14055.

[8] B. Zheng, M. P. von See, E. Yu, B. Gunel, K. Lu, T. Vazin, D. V. Schaffer, P. W. Goodwill, and S. M. Conolly. Quantitative Magnetic Particle Imaging Monitors the Transplantation, Biodistribution, and Clearance of Stem Cells In Vivo. *Theranostics*, 6(3):291–301, 2016, doi:10.7150/thno.13728.

[9] D. Eberbeck, F. Wiekhorst, S. Wagner, and L. Trahms. How the size distribution of magnetic nanoparticles determines their magnetic particle imaging performance. *Applied Physics Letters*, 98(18):182502, 2011, doi:10.1063/1.3586776.

[10] D. Eberbeck, C. L. Dennis, N. F. Huls, K. L. Krycka, C. Gruttner, and F. Westphal. Multicore Magnetic Nanoparticles for Magnetic Particle Imaging. *IEEE Transactions on Magnetics*, 49(1):269–274, 2013, doi:10.1109/TMAG.2012.2226438.

[11] C. McFadden, C. L. Mallett, and P. J. Foster. Labeling of multiple cell lines using a new iron oxide agent for cell tracking by MRI. *Contrast Media & Molecular Imaging*, 6(6):514–522, 2011, doi:10.1002/cmmi.456.

[12] A. Rose, Human Vision, in *Vision*, Boston, MA: Springer US, 1973, 29–53. doi:10.1007/978-1-4684-2037-1_2.

[13] O. C. Sehl, J. J. Gevaert, K. P. Melo, N. N. Knier, and P. J. Foster. A Perspective on Cell Tracking with Magnetic Particle Imaging. *Tomography*, 6(4):315–324, 2020, doi:10.18383/j.tom.2020.00043.

[14] A. S. Arbab, G. T. Yocum, H. Kalish, E. K. Jordan, S. A. Anderson, A. Y. Khakoo, E. J. Read, and J. A. Frank. Efficient magnetic cell labeling with protamine sulfate complexed to ferumoxides for cellular MRI. *Blood*, 104(4):1217–1223, 2004, doi:10.1182/blood-2004-02-0655.

[15] Z. W. Tay, D. W. Hensley, E. C. Vreeland, B. Zheng, and S. M. Conolly. The relaxation wall: experimental limits to improving MPI spatial resolution by increasing nanoparticle core size. *Biomedical Physics & Engineering Express*, 3(3):035003, 2017, doi:10.1088/2057-1976/aa6ab6.

[16] T. Yoshida, N. B. Othman, and K. Enpuku. Characterization of magnetically fractionated magnetic nanoparticles for magnetic particle imaging. *Journal of Applied Physics*, 114(17):173908, 2013, doi:10.1063/1.4829484.

[17] N. Löwa, P. Knappe, F. Wiekhorst, D. Eberbeck, A. F. Thünemann, and L. Trahms. Hydrodynamic and magnetic fractionation of superparamagnetic nanoparticles for magnetic particle imaging. *Journal of Magnetism and Magnetic Materials*, 380:266–270, 2015, doi:10.1016/j.jmmm.2014.08.057.

[18] A. F. Thünemann, S. Rolf, P. Knappe, and S. Weidner. In Situ Analysis of a Bimodal Size Distribution of Superparamagnetic Nanoparticles. *Analytical Chemistry*, 81(1):296–301, 2009, doi:10.1021/ac802009q.

[19] H. Suzuka, A. Mimura, Y. Inaoka, and K. Murase. Magnetic Nanoparticles in Macrophages and Cancer Cells Exhibit Different Signal Behavior on Magnetic Particle Imaging. *Journal*

of Nanoscience and Nanotechnology, 19(11):6857–6865, 2019, doi:10.1166/jnn.2019.16619.

[20] H. Arami and K. M. Krishnan. Intracellular performance of tailored nanoparticle tracers in magnetic particle imaging. *Journal of Applied Physics*, 115(17):17B306, 2014, doi:10.1063/1.4867756.

[21] H. Arami, R. M. Ferguson, A. P. Khandhar, and K. M. Krishnan. Size-dependent ferrohydrodynamic relaxometry of magnetic particle imaging tracers in different environments. *Medical Physics*, 40(7):071904, 2013, doi:10.1118/1.4810962.

[22] J. A. Mindell. Lysosomal Acidification Mechanisms. *Annual Review of Physiology*, 74(1):69–86, 2012, doi:10.1146/annurev-physiol-012110-142317.

[23] M. Levy, N. Luciani, D. Alloyeau, D. Elgrabli, V. Deveaux, C. Pechoux, S. Chat, G. Wang, N. Vats, F. Gendron, C. Factor, S. Lotersztajn, A. Luciani, C. Wilhelm, and F. Gazeau. Long term in vivo biotransformation of iron oxide nanoparticles. *Biomaterials*, 32(16):3988–3999, 2011, doi:10.1016/j.biomaterials.2011.02.031.

[24] E. Teeman, C. Shasha, J. E. Evans, and K. M. Krishnan. Intracellular dynamics of superparamagnetic iron oxide nanoparticles for magnetic particle imaging. *Nanoscale*, 11(16):7771–7780, 2019, doi:10.1039/C9NR01395D.

[25] D. E. Markov, H. Boeve, B. Gleich, J. Borgert, A. Antonelli, C. Sfara, and M. Magnani. Human erythrocytes as nanoparticle carriers for magnetic particle imaging. *Physics in Medicine and Biology*, 55(21):6461–6473, 2010, doi:10.1088/0031-9155/55/21/008.

[26] J. A. Frank, B. R. Miller, A. S. Arbab, H. A. Zywicke, E. K. Jordan, B. K. Lewis, L. H. Bryant, and J. W. M. Bulte. Clinically Applicable Labeling of Mammalian and Stem Cells by Combining Superparamagnetic Iron Oxides and Transfection Agents. *Radiology*, 228(2):480–487, 2003, doi:10.1148/radiol.2281020638.

[27] A. S. Arbab, G. T. Yocum, L. B. Wilson, A. Parwana, E. K. Jordan, H. Kalish, and J. A. Frank. Comparison of Transfection Agents in Forming Complexes with Ferumoxides, Cell Labeling Efficiency, and Cellular Viability. *Molecular Imaging*, 3(1):153535002004031, 2004, doi:10.1162/15353500200403190.

[28] J. J. Gevaert, C. Fink, J. D. Dikeakos, G. A. Dekaban, and P. J. Foster. Magnetic Particle Imaging Is a Sensitive In Vivo Imaging Modality for the Detection of Dendritic Cell Migration. *Molecular Imaging and Biology*, 2022, doi:10.1007/s11307-022-01738-w.

[29] H. Paysen, N. Loewa, A. Stach, J. Wells, O. Kosch, S. Twamley, M. R. Makowski, T. Schaeffter, A. Ludwig, and F. Wiekhorst. Cellular uptake of magnetic nanoparticles imaged and quantified by magnetic particle imaging. *Scientific Reports*, 10(1):1922, 2020, doi:10.1038/s41598-020-58853-3.

[30] J. Rahmer, A. Halkola, B. Gleich, I. Schmale, and J. Borgert. First experimental evidence of the feasibility of multi-color magnetic particle imaging. *Physics in Medicine and Biology*, 60(5):1775–91, 2015, doi:10.1088/0031-9155/60/5/1775.

